Aberrant cohesin function in *Saccharomyces cerevisiae* activates Mcd1 degradation to promote cell lethality

Running title: A cohesin surveillance mechanism

Gurvir Singh[1] and Robert V. Skibbens[1]*.

[1]Department of Biological Sciences, Lehigh University, 111 Research Drive, Bethlehem, Pennsylvania, 18015. United States of America.

* Corresponding author: Robert V. Skibbens, rvs3@lehigh.edu

Key words: Cohesins; Eco1/Ctf7/ESCO2; Rad61/WAPL; Mcd1/Scc1/RAD21; Roberts Syndrome (RBS); Cornelia de Lange Syndrome (CdLS), E3 ligase, San1, Das1, Checkpoints, sister chromatid cohesion, chromosome condensation

ABSTRACT

The cohesin complex is composed of core ring proteins (Smc1, Smc3 and Mcd1) and associated factors (Pds5, Scc3, and Rad61) that bind via Mcd1. Cohesin extrusion (looping from within a single DNA molecule) and cohesion (the tethering together of two different DNA molecules) underlie the many roles that cohesins play in chromosome segregation, gene transcription, DNA repair, chromosome condensation, replication fork progression, and genomic organization. While cohesin function flanks the activities of critical cell checkpoints (including spindle assembly and DNA damage checkpoints), the extent to which cells directly target cohesins in response to aberrant cohesin function remains unknown. Based on prior evidence that cells mutated for cohesin contain reduced Mcd1 protein, we tested whether loss of Mcd1 is based simply on cohesin instability. We find that Mcd1 loss persists even in *rad61* cells, which contain elevated levels of stable chromosome-bound cohesins, contrary to a simple instability model. In fact, re-elevating Mcd1 levels suppressed the temperature-sensitive growth defects of all cohesin alleles tested, revealing that Mcd1 loss is a fundamental mechanism through which cohesins are inactivated to promote cell lethality. Our findings further reveal that cells that exhibit aberrant cohesin function employ E3 ligases to target Mcd1 for degradation. This mechanism of degradation appears unique in that Mcd1 is reduced during S phase, when Mcd1 levels typically peak and despite a dramatic upregulation in *MCD1* transcription. We infer from these latter findings that cells contain a negative feedback mechanism used to maintain Mcd1 homeostasis.

AUTHOR SUMMARY

Cohesins are central to almost all aspects of DNA regulation (chromosome segregation, gene transcription, DNA repair, chromosome condensation, replication fork progression, and genomic organization). Cohesin also play key roles in cell checkpoints: cohesin mutations activate the spindle assembly checkpoint while double strand DNA breaks can elicit a new round of cohesin establishment. In the current study, we provide evidence for a novel cohesin surveillance system that employs E3 ligases that directly target Mcd1, a core component of the cohesin ring structure, for degradation during S phase. We further describe a feedback mechanism through which cells dramatically induce *MCD1* transcription to maintain Mcd1 homeostasis. Finally, we provide evidence that requires the re-evaluation of phenotypes associated with other cohesin gene mutations.

INTRODUCTION

The identification of checkpoints has produced significant clinical advances over the last half century (1, 2). After the discovery that the tumor suppressor p53 is mutated in more than 50% of all cancers, advances from both basic science and clinical settings led to new strategies through which p53 can be re-activated, mutated p53 degraded, or synthetic lethal mechanisms to eliminate cancer cells (3–7). Similarly, highly proliferative cancer cells are disproportionally sensitive to spindle assembly checkpoint inhibitors, compared to non-tumorigenic cells (8–10). Often, factors that exhibit multiple functions, or reside at the nexus of critical pathways, are monitored by surveillance mechanisms and provide important avenues to improve human health.

Cohesins are ATPase protein complexes composed of a core ring (Smc1, Smc3 and Mcd1) and associated factors (Pds5, Scc3, and Rad61) that bind via Mcd1. Cohesins are central to almost all aspects of DNA regulation (chromosome segregation, gene transcription, DNA repair, chromosome condensation, replication fork progression, and genomic organization)(11–28). Underlying this complex output of roles, cohesins perform two essential functions: extrusion (looping from within a single DNA molecule) and cohesion (the tethering together of two different DNA molecules) (11, 12, 16, 17, 21–23). Mutations in cohesins that affect DNA looping can give rise to severe developmental abnormalities such as Cornelia De Lange Syndrome (CdLS) and Roberts Syndrome (RBS). These multifaceted maladies often include intellectual disabilities, hearing loss, microcephaly, phocomelia and abnormalities in the heart and gastrointestinal tract (29–35). Mutations that impact tethering give rise to aneuploidy - a

74 hallmark of cancer cells(36–38). Recent evidence indeed suggests that cancer cells rely
75 on elevated cohesin activity for survival (39–43).

76 It is well established that cohesin functions flank critical cell checkpoints. For
77 instance, cohesin mutations that abolish sister chromatid cohesion (tethering) activate
78 the spindle assembly checkpoint (44–46), consistent with classic micromanipulation and
79 laser ablation studies that cells monitor chromosome biorientation, and thus tension,
80 produced across the two mitotic half-spindles (47–52). In contrast, double strand DNA
81 breaks activate ATM/ATR and CHK1 kinases that elicit a *de novo* round of cohesin
82 deposition and cohesion establishment both at sites of damage and genome-wide (13,
83 19, 53–59). The remarkable involvement of cohesins in cell cycle checkpoints, both to
84 maintain euploidy and promote error-free DNA damage repair, underscores their central
85 role in maintaining genome integrity.

86 In this study, we present evidence that cohesins are a direct target of a
87 surveillance system that may cull aneuploid or transcriptionally aberrant cells from a
88 normal population. The current study was motivated, in part, by previously unexplained
89 observations that cohesin mutations result in a significant reduction of Mcd1 protein
90 (60–63). Rad61 (or the human homolog WAPL) promotes cohesin dissociation from
91 DNA, such that cells with reduced Rad61/WAPL activity contain elevated levels of
92 stable chromosome-bound cohesins, prematurely condensed (and even hyper-
93 condensed) chromatin (64–69). Despite this hyperstabilization of cohesin complexes,
94 our results reveal that Mcd1 is significantly reduced in *rad61* deleted cells. The
95 reduction of Mcd1 in the absence of a temperature-sensitive cohesin allele, and during
96 S phase when Mcd1 levels typically peak, argue against a simple model that cohesin

97 instability accounts for Mcd1 loss. Intriguingly, *MCD1* transcription is dramatically
98 upregulated during S phase despite the reduction in Mcd1 protein levels, suggesting
99 that a novel feedback mechanism typically is in place to maintain Mcd1 homeostasis.
100

101 RESULTS

102 **Rad61 positively regulates cohesins through Mcd1**

103 The majority of cohesin-mutated cells tested to date (*smc1-259*, *smc3-42*, *pds5-*
104 *1*, *pds5Δ elg1Δ*, and *eco1Δ rad61Δ*) contain significantly reduced levels of Mcd1 protein
105 (60–63). Rad61 dissociates cohesin from DNA such that *rad61Δ* cells retain elevated
106 levels of stably-bound cohesins (65–73). Given the opposing activities of Eco1 (cohesin
107 stabilization) and Rad61 (cohesin dissociation), we hypothesized that *rad61Δ* cells
108 should retain wildtype levels of Mcd1 and suppress the loss of Mcd1 in *eco1* mutated
109 cells. To test these predictions, log phase cultures of wildtype, *rad61Δ*, *eco1-203*, and
110 *eco1Δ rad61Δ* cells were arrested in early S phase (hydroxyurea, HU) prior to shifting to
111 37°C (Figure 1A). Surprisingly, Western blot quantifications of the resulting mitotic
112 extracts revealed that Mcd1 levels are reduced not only in *eco1* temperature-sensitive
113 (ts) strains, but also significantly reduced in *rad61Δ* cells (Figures 1B, 1C). Nor did the
114 deletion of *RAD61* provide any benefit to *eco1Δ* cells with respect to Mcd1 levels
115 (Figures 1B, 1C). These results suggest that Mcd1 levels may be reduced by a
116 surveillance system that monitors for aberrant cohesin function beyond cohesin
117 complex stability.
118

A negative feedback loop regulates *MCD1* expression

The near ubiquitous reduction of Mcd1 in cohesin-mutated cells prompted us to uncover the underlying molecular mechanism. Mcd1 is unique among cohesin subunits in that it is the only core subunit that is degraded at anaphase onset (to allow for sister chromatid segregation), and then transcribed starting at the G1/S transition, each and every cell cycle (11, 62, 74). Previous findings documented a complex transcriptional network that regulates *MCD1* expression (61). It thus became important to test the extent to which *MCD1* transcription is reduced in the *eco1Δ rad61Δ* cells. Log phase wildtype and *eco1Δ rad61Δ* cells were arrested in early S phase (HU, hydroxyurea) (Figure 2A) - a point in the cell cycle at which *MCD1* expression and Mcd1 protein levels peak in wildtype cells, but in which Mcd1 protein levels are significantly reduced in *eco1Δ rad61Δ* cells (11, 61). We confirmed that Mcd1 protein levels were significantly reduced in the same *eco1 rad61* cultures (Figures 2B, 2C) used to test for changes in *MCD1* transcription. In contrast to the model that *MCD1* transcription is decreased, quantification of qRT-PCR revealed that *MCD1* transcript levels are instead significantly increased (~5.5 fold) in *eco1Δ rad61Δ* cells compared to wildtype cells (Figure 2D). These results indicate that the loss of Mcd1 protein in *eco1Δ rad61Δ* cells is not dependent on reduced *MCD1* transcription. Moreover, our findings reveal a compensatory feedback mechanism in which cells increase *MCD1* transcription in response to decreased Mcd1 protein levels.

An E3 ligase mechanism promotes Mcd1 degradation

141 Having excluded a transcription-based mechanism, it became important to test
142 the extent to which the reduction in Mcd1 protein level occurs through degradation.
143 Mcd1 is reduced in early S phase in *eco1Δ rad61Δ* cells, suggesting that a degradation
144 mechanism is likely independent of Esp1, a caspase-type protease that cleaves Mcd1
145 during anaphase onset (61, 74–76). To formally test this hypothesis, *eco1Δ rad61Δ* cells
146 and *esp1-1* cells were mated and the resulting diploids sporulated and dissected.
147 Reduced Esp1 activity, however, failed to suppress *eco1Δ rad61Δ* cells ts growth
148 defects (data not shown), consistent with a role for Esp1 that is predominantly limited to
149 mitosis (74, 76).
150 Protein ubiquitination, through E3 ligases, play key roles in numerous cellular
151 activities that include degradation (77, 78). Thus, we focused on E3 ligases as a
152 mechanism required to reduce Mcd1 protein levels, a model supported by prior
153 evidence that Mcd1 is a target of ubiquitination (79, 80). The E3 ligases that target
154 Mcd1 remained unidentified, requiring us to generate a candidate list based on genetic
155 or physical interactions (BioGrid and SGD) across various cohesins subunits (81–84).
156 We prioritized our efforts on five candidates (Bre1, Bul2, Lbd19, Das1, and San1), all of
157 which are encoded by non-essential genes. We reasoned that if any of the candidates
158 E3 ligases are in part responsible for ubiquitinating Mcd1, then their deletion should
159 suppress *eco1Δ rad61Δ* cell ts growth defects. To test this model, each of the E3 ligases
160 genes (*BRE1*, *BUL2*, *LBD19*, *DAS1* and *SAN1*) were individually deleted from wildtype
161 and *eco1Δ rad61Δ* cells. Log phase cultures of the resulting transformants were serially
162 diluted onto rich medium plates and incubated at either 30°C or 37°C, temperatures
163 respectively permissive and non-permissive for *eco1Δ rad61Δ* cell growth (Figure 3).

164 Deletion of *BUL2* had no impact on either wildtype or *eco1Δ rad61Δ* cells at either
165 temperature (Figure 3A). Deletion of *BRE1* exhibited an adverse effect on both wildtype
166 and *eco1Δ rad61Δ* cells (Figure 3B), consistent with a prior report that *bre1Δ* cells
167 exhibit genomic instability (85). Compared to the adverse but non-specific impact of
168 *BRE1* deletion, deletion of *LBD19* produced a severe negative impact specific to *eco1Δ*
169 *rad61Δ* cells (Figure 3C). In contrast to the results above, deletion of *SAN1*, and to a
170 lesser extent *DAS1*, suppressed the ts growth defects otherwise exhibited by *eco1Δ*
171 *rad61Δ* cells (Figure 3D, 3E). Thus, E3 ligases San1 and Das1 play critical roles in
172 Mcd1 degradation in response to reduced cohesin function.
173

174 *MCD1* overexpression rescues the inviabilty of cohesin mutated cells

175 The reduction in Mcd1 protein levels is an attribute common to all cohesin-
176 mutated cells tested to date (60–63, this study). This near ubiquitous reduction in Mcd1
177 prompted us to ask the following question: are cohesin mutated cell ts-lethalities due to
178 the mutated cohesin allele (ie. Mcd1 loss is a downstream consequence of cohesin
179 inactivation, but otherwise unimportant) or due to the reduction in Mcd1? To
180 differentiate between these two possibilities, we tested the extent to which elevated
181 expression of *MCD1* could suppress the lethality of cells that harbor ts mutations in
182 other cohesin genes. Wildtype, *eco1-1*, *scc3-6*, *smc3-42*, and *smc1-259* cells were each
183 transformed with either vector alone or vector driving elevated expression of *MCD1* and
184 log phase culture of the resulting transformants serially diluted onto selective media
185 plates. As expected, elevated *MCD1* expression had no effect on the growth of wildtype
186 cells at the temperatures tested. In contrast, overexpression of *MCD1* suppressed the ts

187 growth defects in all five cohesin ts alleles (Figure 4) - in some cases up to the elevated
188 temperature of 37°C. We further found that elevated *MCD1* expression suppressed the
189 ts growth defect of *scc2-4* mutant cells in which mutation of a cohesin subunits is fully
190 absent (Figure 4E). These results not only provide evidence that loss of Mcd1
191 significantly contributes to the lethality of cohesin-mutated cells, but also confound prior
192 interpretations of the severity of phenotypes attributed solely to those ts alleles.
193

194 **Mcd1 differentially contributes to cohesion and condensation**

195 Above, we established Mcd1 as a key driver of most, if not all, cohesin-mutated
196 strain lethalities. It next became important to test which if any cohesin functions are
197 rescued by elevated Mcd1 levels in cells that harbor mutation in another cohesin gene.
198 Wildtype and *smc1-259* strains were genetically modified to contain either an rDNA
199 condensation marker (Net1-GFP) or a cohesion assay cassette (tetO and TetR-GFP)
200 (11, 12, 20, 69, 72, 86, 87). The modified strains were then transformed with a high-
201 copy vector alone or vector that drives elevated expression of *MCD1*. Log phase
202 cultures of the resulting transformants were arrested in G1 (alpha factor, αF) and then
203 released into 34°C (non-permissive for *smc1-259* cells) rich medium that contains
204 nocodazole (NZ) to arrest cells in preanaphase. DNA content (flow cytometry) and cell
205 morphologies were monitored at various stages of both experiments (Figures 5A, 6A).
206 Notably, *smc1-259* mutant cells have not been previously assessed for
207 condensation defects. Here, we exploited the well-established analysis of rDNA
208 chromatin architecture using Ne1-GFP (11, 20, 69, 72, 88). In wildtype cells, rDNA
209 converts from a decondensed puff-like structure during G1 into tight loops (occasionally

210 observed as bars) during mitosis (89). As expected, wildtype cells arrested in
211 preanaphase exhibited well-defined rDNA loops, indicative of robust chromosome
212 condensation (Figure 5B, 5C). In contrast, only 21% of *smc1-259* cells contained tight
213 loops such that the majority of cells exhibited defects in rDNA condensation (Figure 5B,
214 5C). These results extend prior findings regarding the condensation defects exhibited by
215 other cohesin mutated strains (11, 28, 44, 71, 90–92). Elevated expression of *MCD1*
216 had no observable impact on rDNA structure in wildtype cells. Surprisingly, *MCD1*
217 expression produced only a modest increase (38%, compared to 21% in the vector
218 control) in the percent of *smc1-259* cells that contained condensed rDNA loops (Figure
219 5C). Given prior evidence that suppression of condensation defects underlies the
220 improved viability of cohesin-mutated cells (93), we decided to further investigate the
221 condensation of rDNA structure. Mutated cells that did not contain tight and well-defined
222 rDNA loops were parsed into two categories: puff-like (fully decondensed) and in which
223 some structure was apparent within the rDNA mass (partial decondensation). Focusing
224 on the more severe of the two phenotypes, *smc1-259* cells that contained vector alone
225 were strongly biased toward the frequency of puffs (~65% puffs compared to 12%
226 partial condensed) (Figure 5D). *smc1-259* cells in which *MCD1* was over expressed,
227 however, contained a significant decrease in the frequency of puffs (25%, down from
228 65% for vector alone) (Fig 5D). In combination, these findings reveal that Mcd1 exerts a
229 relatively limited impact on rDNA condensation.

230 Next, we assessed the effect of elevated *MCD1* expression on sister chromatid
231 cohesion. In wildtype cells, the GFP-marked tetO that marks each sister chromatid are
232 closely tethered together to appear as a single dot. In cohesin mutated cells, the

233 separated sisters are readily detected as two dots (12). Elevated expression of *MCD1*
234 had no effect on sister chromatid cohesion such that wildtype cells contained very high
235 frequencies of tethered sister chromatids (1 dot/nucleus), regardless of harboring vector
236 alone or vector expressing *MCD1* (Figure 6). *smc1-259* cells that contained vector alone
237 exhibited a high (60%) frequency of 2 dots/nucleus (Figure 6), consistent with prior
238 studies and the frequency of cohesion defects observed in other cohesin mutated cells
239 (11, 44, 90, 91, 93, 94). Notably, elevated expression of *MCD1* significantly restored
240 sister chromatid tethering in *smc1-259* cells, with only 35% (compared to 60% vector
241 control) of cells exhibiting cohesion defects. Thus, elevated *MCD1* expression is
242 sufficient to elicit a robust rescue in cohesion, but not condensation, defects. More
243 importantly, cell defects in condensation, compared to cohesion, appear largely
244 attributable to the *smc1-259* allele.
245

246 DISCUSSION

247 The core cohesin component, Mcd1, which caps the ATPase domains of Smc1 and
248 Smc3 in core cohesin complexes, is greatly reduced in cells that harbor mutations in
249 nearly every cohesin gene tested to date (60–63, this study). A priori, a simple
250 explanation is that cohesin gene mutations destabilize the cohesin ring and, in some
251 fashion, promote the loss of the non-mutated Mcd1 protein. The first revelation of the
252 current study is that Mcd1 is significantly reduced in *rad61Δ* strains - cells in which
253 cohesins appear hyper-stabilized, exhibit extended DNA-association and exhibit
254 increased cohesin activities that include chromosome compaction and DNA loop
255 formation (61, 65–69, 71–73, 95, 95). Moreover, Mcd1 is reduced in the absence of

256 elevated temperatures (*eco1 rad61*), in the absence of a ts cohesin allele (*rad61*), and
257 re-elevating Mcd1 levels suppresses the ts growth defects of cells that harbor no
258 cohesin subunit allele (*scc2-4*). These findings, coupled with the recognition that it is
259 wildtype Mcd1 protein that is reduced, rather than a mutated or misfolded version, are
260 inconsistent with a simple instability model.

261 What signals Mcd1 degradation? It is tempting to speculate that cells respond to
262 defective or aberrant cohesin functions by activating a unique mechanism to cull out
263 cells that might otherwise contribute to an aneuploid or developmentally-altered
264 population. Mcd1 targeting may not be exclusive to cells that incur cohesin defects
265 given that exposure to reactive oxygen species also triggers Mcd1 degradation in an
266 apoptotic response that includes the caspase-like Esp1 (96–99). The conserved nature
267 of this targeting mechanism is further supported by findings that RAD21 (homolog of
268 Mcd1) is degraded by caspases 3 and 7 during apoptotic responses (96, 100, 101).
269 Together, these results suggest that inactivating cohesin functions through Mcd1
270 degradation may represent an evolutionarily conserved mechanism for promoting cell
271 death.

272 The second set of findings that emerge from the current study is the identification of
273 the pathway through which Mcd1 is degraded. In unperturbed cells, Mcd1 is degraded
274 at anaphase onset by Esp1. Here, our findings largely negate a role for an Esp1-
275 dependent mechanism during S phase and instead document novel roles for E3 ligases
276 (San1 and Das1) in promoting Mcd1 degradation during S phase, a time when Mcd1
277 levels typically peak. How information that arises from cohesin defects might be relayed
278 to E3 ligases remains unknown. Recent evidence, however, suggests that the Cln2-

279 containing G1 CDK plays a critical role. For instance, deletion of *CLN2* rescues both
280 *eco1 rad61* cell ts growth defects and *pds5 elg1* lethality - both through increased Mcd1
281 levels (60, 68). These findings support a mechanism in which cohesin defects (or
282 aberrant functioning) from the prior cell cycle activate Cln2-CDK to promote E3 ligase-
283 dependent degradation of Mcd1. It will be important to test whether these preceding
284 defects might include retention of an activated spindle checkpoint (due to cohesion
285 defects) or transcriptional abnormalities that arise due to defects in cohesin extrusion
286 activities.

287 The findings reported here impact all prior analyses of cohesin mutated strains. The
288 lethality of mutated cohesin strains alleles were interpreted to reflect protein
289 inactivation/misfolding of the mutated protein. Instead, we find substantial suppression
290 of the ts growth defects that occur in cohesin mutated cells (*smc1*, *smc3*, *scc3*, *scc2*
291 and *eco1*) simply by re-elevating Mcd1 levels. Previously, the severity of cohesin
292 phenotypes (loss of sister chromatid cohesion, defects in chromosome condensation,
293 and genotoxic sensitivities) were found to scale closely to changes in Mcd1 levels (102).
294 We were thus intrigued by the possibility that elevated *MCD1* might differentially
295 suppress phenotypes otherwise exhibited by cohesin mutated strains. Indeed, our
296 findings reveal that re-elevating Mcd1 produces a more robust rescue of cohesion
297 defects, compared to the rescue of condensation defects in *smc1-259* cells. We infer
298 from these findings that Mcd1-dependent restoration of cohesion primarily accounts for
299 the decrease in temperature-sensitive growth of *smc1-259* cells. These results further
300 reveal that Smc1 appears to have a greater role in condensation, compared to
301 cohesion, than previously reported. In combination, these findings suggest that a re-

302 evaluation regarding the severity of associated alleles is warranted. More broadly,
303 studies that characterize phenotypes for a mutated component within a complex should
304 be coupled with analyses regarding the persistence of the remaining subunits.

305 The final revelation of the current study relates to the mechanism through which
306 yeast cells achieve homeostatic levels of Mcd1. Subsequent to degradation at
307 anaphase onset, Mcd1 levels rise starting at the G1/S transition and peak during S
308 phase. Our results suggest that Mcd1 protein negatively regulates its own expression
309 such that E3-ligase degradation Mcd1 results in a dramatic upregulation in *MCD1*
310 expression during S phase. Notably, the balance heavily favors degradation over
311 transcription, suggesting that E3 ligases become significantly activated (compared to
312 the approximately 5.5-fold increase in *MCD1* transcription) in response to cohesin
313 defects.
314

315 MATERIALS AND METHODS

316 **Yeast strains, media, and growth conditions**: All strains (see Supplementary
317 Table 1 for strain genotypes) were grown on YPD-rich media unless placed on selective
318 medium to facilitate plasmid transformation/retention or spore identification (103).
319 **Strain generation**: Primers used to delete genes (*BUL2*, *BRE1*, *LBD19*, *DAS1*
320 and *SAN1*) and verify proper integration are listed in Supplementary Table 2. GFP-
321 tagging Net1, to include either *kanMX6* or *TRP1* markers, are previously described
322 (104). The cohesion assay strains used in this study (YGS333, YGS334, YGS321,
323 YGS323) were generated by crossing *smc1-259* (YBS3168/ K6013) with wildtype cells
324 that harbor the cohesion assay cassette (*tetO:URA3 tetR-GFP:LEU2 Pds1-Myc:TRP1*)

325 (YBS1042) (87, 105). The resulting diploid (YGS301) was sporulated and dissected to
326 obtain *smc1-259 tetO:URA3 tetR-GFP:LEU2* cells and wildtype cassette strain
327 *tetO:URA3 tetR-GFP:LEU2*.

328 Wildtype and cohesin mutant cells overexpressing vector were transformed with
329 either pRS424 plasmid (2μ *TRP1*) or pRS425 (2μ *LEU*) and cells overexpressing *MCD1*
330 were transformed either with pRS425 (2μ *LEU*) or pGS35 (2μ *LEU2 MCD1*) (61). See
331 Supplementary Table 1 for resulting strain names and genotypes.

332 **Western Blots**: Cell numbers for each log phase strain were normalized to 2
333 OD_{600}. Whole cell protein extracts were prepared as described in (106) with minor
334 modifications. Cells were mechanically lysed (Bead-beater, BioSpec) in 17% TCA with
335 regular intermittent cooling on ice. The beads were washed two times in 500μL of 5%
336 TCA and the two lysates combined and centrifuged at 15,000 rpm for 20 min at 4°C with
337 subsequent solubilization in 3% SDS and 0.25 M Tris-base buffer. Western blotting and
338 protein detection using the anti-Mcd1 antibody (generous gift from Dr. Vincent Guacci),
339 anti-PGK1 (Invitrogen), Goat anti-Mouse HRP (BIO-RAD) or Goat anti-Rabbit HRP
340 (BIO-RAD), were performed as previously described (61). Protein band intensities
341 (obtained by ChemiDoc™ MP) were quantified using Image J. Significance was
342 determined by a two-tailed test as described in legends.

343 **RNA extraction and qRT-PCR:** Cell numbers from log phase cultures were
344 normalized to 2 OD_{600} , pelleted by centrifugation and frozen in liquid nitrogen. Cells
345 were lysed mechanically using a bead-beater (BioSpec) for 8 min with intermittent
346 cooling on ice. RNA was extracted and purified using the RNeasy Mini Kit (Qiagen) per
347 manufacturer's instructions and quantified using a nanodrop (Thermo Scientific,

348 NanoDrop One^{C}). Normalized RNAs were treated with Turbo DNase (Ambion) and then
349 reverse transcribed using SupercriptIII (Invitrogen). Quantitative Real -Time (qRT) PCR
350 was performed in triplicates using the Rotor-Gene SYBR Green PCR kit (Cat. No.
351 204074) and C_T values measured using the Rotor Gene (Corbett). C_T values of *MCD1*
352 and internal control ALG9 were averaged and the fold change in *MCD1* expression
353 determined using the $2^{-\Delta\Delta Ct}$method (107).

354 **Condensation and Cohesion Assays**: Cohesion and condensation assays
355 were performed as previously described (86) with the following modifications. Log
356 phase cells were grown in selective media, followed by pre-synchronized in G1 (alpha
357 factor) for 3 hr at 23°C in YPD- rich media. The resulting cultures were harvested,
358 washed 2 times and then shifted to 37°C for 3 hr in fresh media supplemented with
359 nocodazole. Cell aliquots of the resulting preanaphase arrested cells were fixed at room
360 temperature in paraformaldehyde to a final concentration of 3.7%. Cells were assayed
361 using an E800 light microscope (Nikon) equipped with a cooled CD camera
362 (Coolsnapfx, Photometrics) and imaging software (IPLab, Scanalytics).

363 **Flow Cytometry and Cell Cycle Progression**: Log phase cultures were
364 normalized (OD_{600}) and synchronized at specific cell stages using the following
365 treatments: early S phase with 0.2 M Hydroxyurea (SIGMA, H8627), G1 phase with 3
366 μM alpha factor (ZYMO RESEARCH, Y1001), M phase with 20 μg/ml of nocodazole
367 (SIGMA, M1404). Log phase growth and proper cell cycle arrest were confirmed by flow
368 cytometry as previously described (86, 95).

369

370 # ACKNOWLEDGEMENTS

The authors gratefully acknowledge the generous gifts of Mcd1-directed antibody and numerous yeast strains from Dr. Vincent Guacci and the Koshland Lab. The authors also Skibbens lab members and participants in the Super Group Yeast Club for helpful discussions during the preparation of this paper.

REFERENCES

1. L. H. Hartwell, T. A. Weinert, Checkpoints: Controls That Ensure the Order of Cell Cycle Events. *Science* **246**, 629–634 (1989).
2. R. Uzbekov, C. Prigent, A Journey through Time on the Discovery of Cell Cycle Regulation. *Cells* **11**, 704 (2022).
3. M. Masutani, T. Nozaki, K. Wakabayashi, T. Sugimura, Role of poly(ADP-ribose) polymerase in cell-cycle checkpoint mechanisms following γ-irradiation. *Biochimie* **77**, 462–465 (1995).
4. S. Tsukamoto, Natural products that target p53 for cancer therapy. *J Nat Med* **79**, 725–737 (2025).
5. S. Nishikawa, T. Iwakuma, Drugs Targeting p53 Mutations with FDA Approval and in Clinical Trials. *Cancers* **15**, 429 (2023).
6. W. Li, F. Wang, R. Guo, Z. Bian, Y. Song, Targeting macrophages in hematological malignancies: recent advances and future directions. *J Hematol Oncol* **15** (2022).
7. P. Baliakas, T. Soussi, The TP53 tumor suppressor gene: From molecular biology to clinical investigations. *J Intern Med* **298**, 78–96 (2025).

8. B. A. A. Weaver, D. W. Cleveland, Decoding the links between mitosis, cancer, and chemotherapy: The mitotic checkpoint, adaptation, and cell death. *Cancer Cell* **8**, 7–12 (2005).

9. K. Tanaka, T. Hirota, Chromosome segregation machinery and cancer. *Cancer Science* **100**, 1158–1165 (2009).

10. J. Gallego-Jara, G. Lozano-Terol, R. A. Sola-Martínez, M. Cánovas-Díaz, T. De Diego Puente, A Compressive Review about Taxol®: History and Future Challenges. *Molecules* **25**, 5986 (2020).

11. V. Guacci, D. Koshland, A. Strunnikov, A Direct Link between Sister Chromatid Cohesion and Chromosome Condensation Revealed through the Analysis of MCD1 in S. cerevisiae. *Cell* **91**, 47–57 (1997).

12. C. Michaelis, R. Ciosk, K. Nasmyth, Cohesins: Chromosomal Proteins that Prevent Premature Separation of Sister Chromatids. *Cell* **91**, 35–45 (1997).

13. C. Sjögren, K. Nasmyth, Sister chromatid cohesion is required for postreplicative double-strand break repair in Saccharomyces cerevisiae. *Current Biology* **11**, 991–995 (2001).

14. R. Jessberger, The many functions of smc proteins in chromosome dynamics. *Nat Rev Mol Cell Biol* **3**, 767–778 (2002).

15. J.-S. Kim, T. B. Krasieva, V. LaMorte, A. M. R. Taylor, K. Yokomori, Specific Recruitment of Human Cohesin to Laser-induced DNA Damage. *Journal of Biological Chemistry* **277**, 45149–45153 (2002).

16. E. de Wit, *et al.*, CTCF Binding Polarity Determines Chromatin Looping. *Molecular Cell* **60**, 676–684 (2015).

416 17. I. F. Davidson, *et al.*, Rapid movement and transcriptional re-localization of human
417 cohesin on DNA. *The EMBO Journal* **35**, 2671–2685 (2016).
418 18. M.-E. Terret, R. Sherwood, S. Rahman, J. Qin, P. V. Jallepalli, Cohesin acetylation
419 speeds the replication fork. *Nature* **462**, 231–234 (2009).
420 19. E. Ünal, J. M. Heidinger-Pauli, D. Koshland, DNA Double-Strand Breaks Trigger
421 Genome-Wide Sister-Chromatid Cohesion Through Eco1 (Ctf7). *Science* **317**, 245–
422 248 (2007).
423 20. T. Hartman, K. Stead, D. Koshland, V. Guacci, Pds5p Is an Essential Chromosomal
424 Protein Required for Both Sister Chromatid Cohesion and Condensation in
425 *Saccharomyces cerevisiae*. *The Journal of Cell Biology* **151**, 613–626 (2000).
426 21. J. H. I. Haarhuis, *et al.*, The Cohesin Release Factor WAPL Restricts Chromatin
427 Loop Extension. *Cell* **169**, 693-707.e14 (2017).
428 22. S. S. P. Rao, *et al.*, Cohesin Loss Eliminates All Loop Domains. *Cell* **171**, 305-
429 320.e24 (2017).
430 23. G. Wutz, *et al.*, Topologically associating domains and chromatin loops depend on
431 cohesin and are regulated by CTCF, WAPL, and PDS5 proteins. *The EMBO*
432 *Journal* **36**, 3573–3599 (2017).
433 24. E. Lara-Pezzi, *et al.*, Evidence of a Transcriptional Co-activator Function of
434 Cohesin STAG/SA/Scc3. *Journal of Biological Chemistry* **279**, 6553–6559 (2004).
435 25. R. A. Rollins, P. Morcillo, D. Dorsett, Nipped-B, a Drosophila Homologue of
436 Chromosomal Adherins, Participates in Activation by Remote Enhancers in the cut
437 and Ultrabithorax Genes. *Genetics* **152**, 577–593 (1999).

438 26. R. A. Rollins, M. Korom, N. Aulner, A. Martens, D. Dorsett, *Drosophila* Nipped-B
439 Protein Supports Sister Chromatid Cohesion and Opposes the Stromalin/Scc3
440 Cohesion Factor To Facilitate Long-Range Activation of the *cut* Gene. *Molecular*
441 *and Cellular Biology* **24**, 3100–3111 (2004).
442 27. R. V. Skibbens, J. Marzillier, L. Eastman, Cohesins coordinate gene transcriptions
443 of related function within*Saccharomyces cerevisiae*. *Cell Cycle* **9**, 1601–1606
444 (2010).
445 28. S. Gard, *et al.*, Cohesinopathy mutations disrupt the subnuclear organization of
446 chromatin. *Journal of Cell Biology* **187**, 455–462 (2009).
447 29. I. D. Krantz, *et al.*, Cornelia de Lange syndrome is caused by mutations in NIPBL,
448 the human homolog of Drosophila melanogaster Nipped-B. *Nat Genet* **36**, 631–635
449 (2004).
450 30. E. T. Tonkin, T.-J. Wang, S. Lisgo, M. J. Bamshad, T. Strachan, NIPBL, encoding a
451 homolog of fungal Scc2-type sister chromatid cohesion proteins and fly Nipped-B,
452 is mutated in Cornelia de Lange syndrome. *Nat Genet* **36**, 636–641 (2004).
453 31. B. Schüle, A. Oviedo, K. Johnston, S. Pai, U. Francke, Inactivating Mutations in
454 ESCO2 Cause SC Phocomelia and Roberts Syndrome: No Phenotype-Genotype
455 Correlation. *The American Journal of Human Genetics* **77**, 1117–1128 (2005).
456 32. H. Vega, *et al.*, Roberts syndrome is caused by mutations in ESCO2, a human
457 homolog of yeast ECO1 that is essential for the establishment of sister chromatid
458 cohesion. *Nat Genet* **37**, 468–470 (2005).
459 33. A. Musio, *et al.*, X-linked Cornelia de Lange syndrome owing to SMC1L1
460 mutations. *Nat Genet* **38**, 528–530 (2006).

461 34. M. A. Deardorff, *et al.*, Mutations in Cohesin Complex Members SMC3 and SMC1A
462 Cause a Mild Variant of Cornelia de Lange Syndrome with Predominant Mental
463 Retardation. *The American Journal of Human Genetics* **80**, 485–494 (2007).
464 35. M. Gordillo, *et al.*, The molecular mechanism underlying Roberts syndrome
465 involves loss of ESCO2 acetyltransferase activity. *Human Molecular Genetics* **17**,
466 2172–2180 (2008).
467 36. J. Antony, C. V. Chin, J. A. Horsfield, Cohesin Mutations in Cancer: Emerging
468 Therapeutic Targets. *Int J Mol Sci* **22**, 6788 (2021).
469 37. M. Di Nardo, M. M. Pallotta, A. Musio, The multifaceted roles of cohesin in cancer.
470 *J Exp Clin Cancer Res* **41**, 96 (2022).
471 38. D. Pati, Role of chromosomal cohesion and separation in aneuploidy and
472 tumorigenesis. *Cell Mol Life Sci* **81**, 100 (2024).
473 39. J. Yun, *et al.*, Reduced cohesin destabilizes high-level gene amplification by
474 disrupting pre-replication complex bindings in human cancers with chromosomal
475 instability. *Nucleic Acids Res* **44**, 558–572 (2016).
476 40. H. Xu, *et al.*, Enhanced RAD21 cohesin expression confers poor prognosis and
477 resistance to chemotherapy in high grade luminal, basal and HER2 breast cancers.
478 *Breast Cancer Res* **13** (2011).
479 41. P. Sarogni, *et al.*, Overexpression of the cohesin-core subunit SMC1A contributes
480 to colorectal cancer development. *J Exp Clin Cancer Res* **38** (2019).
481 42. Y. Huang, *et al.*, ESCO2's oncogenic role in human tumors: a pan-cancer analysis
482 and experimental validation. *BMC Cancer* **24** (2024).

483 43. W. Gan, *et al.*, Prognostic Values and Underlying Regulatory Network of Cohesin
484 Subunits in Esophageal Carcinoma. *J Cancer* **13**, 1588–1602 (2022).
485 44. R. V. Skibbens, L. B. Corson, D. Koshland, P. Hieter, Ctf7p is essential for sister
486 chromatid cohesion and links mitotic chromosome structure to the DNA replication
487 machinery. *Genes & Development* **13**, 307–319 (1999).
488 45. K. Tanaka, *et al.*, Fission Yeast Eso1p Is Required for Establishing Sister
489 Chromatid Cohesion during S Phase. *Molecular and Cellular Biology* **20**, 3459–
490 3469 (2000).
491 46. Md. T. Hoque, F. Ishikawa, Cohesin Defects Lead to Premature Sister Chromatid
492 Separation, Kinetochore Dysfunction, and Spindle-assembly Checkpoint Activation.
493 *Journal of Biological Chemistry* **277**, 42306–42314 (2002).
494 47. X. Li, R. B. Nicklas, Mitotic forces control a cell-cycle checkpoint. *Nature* **373**, 630–
495 632 (1995).
496 48. R. B. Nicklas, How Cells Get the Right Chromosomes. *Science* **275**, 632–637
497 (1997).
498 49. J. Kuhn, S. Dumont, Mammalian kinetochores count attached microtubules in a
499 sensitive and switch-like manner. *Journal of Cell Biology* **218**, 3583–3596 (2019).
500 50. J. R. Aist, H. Liang, M. W. Berns, Astral and spindle forces in PtK2 cells during
501 anaphase B: a laser microbeam study. *Journal of Cell Science* **104**, 1207–1216
502 (1993).
503 51. C. L. Rieder, E. A. Davison, L. C. Jensen, L. Cassimeris, E. D. Salmon, Oscillatory
504 movements of monooriented chromosomes and their position relative to the spindle

505 pole result from the ejection properties of the aster and half-spindle. *The Journal of*
506 *cell biology* **103**, 581–591 (1986).
507 52. R. V. Skibbens, C. L. Rieder, E. D. Salmon, Kinetochore motility after severing
508 between sister centromeres using laser microsurgery: Evidence that kinetochore
509 directional instability and position is regulated by tension. *Journal of Cell Science*
510 **108**, 2537–2548 (1995).
511 53. S.-T. Kim, B. Xu, M. B. Kastan, Involvement of the cohesin protein, Smc1, in Atm-
512 dependent and independent responses to DNA damage. *Genes Dev* **16**, 560–570
513 (2002).
514 54. E. Ünal, *et al.*, DNA Damage Response Pathway Uses Histone Modification to
515 Assemble a Double-Strand Break-Specific Cohesin Domain. *Molecular Cell* **16**,
516 991–1002 (2004).
517 55. L. Ström, H. B. Lindroos, K. Shirahige, C. Sjögren, Postreplicative Recruitment of
518 Cohesin to Double-Strand Breaks Is Required for DNA Repair. *Molecular Cell* **16**,
519 1003–1015 (2004).
520 56. L. Ström, *et al.*, Postreplicative Formation of Cohesion Is Required for Repair and
521 Induced by a Single DNA Break. *Science* **317**, 242–245 (2007).
522 57. X. Kong, *et al.*, Distinct Functions of Human Cohesin-SA1 and Cohesin-SA2 in
523 Double-Strand Break Repair. *Molecular and Cellular Biology* **34**, 685–698 (2014).
524 58. H. Luo, *et al.*, Regulation of Intra-S Phase Checkpoint by Ionizing Radiation (IR)-
525 dependent and IR-independent Phosphorylation of SMC3. *Journal of Biological*
526 *Chemistry* **283**, 19176–19183 (2008).

527 59. E. Watrin, J.-M. Peters, The cohesin complex is required for the DNA damage-
528 induced G2/M checkpoint in mammalian cells. *EMBO J* **28**, 2625–2635 (2009).
529 60. K. Choudhary, *et al.*, S. cerevisiae Cells Can Grow without the Pds5 Cohesin
530 Subunit. *mBio* **13**, e01420-22 (2022).
531 61. G. Singh, R. V. Skibbens, Fdo1, Fkh1, Fkh2, and the Swi6-Mbp1 MBF complex
532 regulate Mcd1 levels to impact eco1 rad61 cell growth in Saccharomyces
533 cerevisiae. *Genetics* **228**, iyae128 (2024).
534 62. A. Toth, *et al.*, Yeast Cohesin complex requires a conserved protein, Eco1p(Ctf7),
535 to establish cohesion between sister chromatids during DNA replication. *Genes &*
536 *Development* **13**, 320–333 (1999).
537 63. L. M. D'Ambrosio, B. D. Lavoie, Pds5 Prevents the PolySUMO-Dependent
538 Separation of Sister Chromatids. *Current Biology* **24**, 361–371 (2014).
539 64. R. Gandhi, P. J. Gillespie, T. Hirano, Human Wapl Is a Cohesin-Binding Protein that
540 Promotes Sister-Chromatid Resolution in Mitotic Prophase. *Current Biology* **16**,
541 2406–2417 (2006).
542 65. S. Kueng, *et al.*, Wapl Controls the Dynamic Association of Cohesin with
543 Chromatin. *Cell* **127**, 955–967 (2006).
544 66. B. D. Rowland, *et al.*, Building Sister Chromatid Cohesion: Smc3 Acetylation
545 Counteracts an Antiestablishment Activity. *Molecular Cell* **33**, 763–774 (2009).
546 67. T. Sutani, T. Kawaguchi, R. Kanno, T. Itoh, K. Shirahige, Budding Yeast
547 Wpl1(Rad61)-Pds5 Complex Counteracts Sister Chromatid Cohesion-Establishing
548 Reaction. *Current Biology* **19**, 492–497 (2009).

549 68. S. Buskirk, R. V. Skibbens, G1-Cyclin2 (Cln2) promotes chromosome
550 hypercondensation in *eco1/ctf7 rad61* null cells during hyperthermic stress in
551 *Saccharomyces cerevisiae*. *G3 Genes|Genomes|Genetics* **12**, jkac157 (2022).
552 69. L. Lopez-Serra, A. Lengronne, V. Borges, G. Kelly, F. Uhlmann, Budding Yeast
553 Wapl Controls Sister Chromatid Cohesion Maintenance and Chromosome
554 Condensation. *Current Biology* **23**, 64–69 (2013).
555 70. M. E. Maradeo, R. V. Skibbens, The Elg1-RFC Clamp-Loading Complex Performs
556 a Role in Sister Chromatid Cohesion. *PLoS ONE* **4**, e4707 (2009).
557 71. C. M. Zuilkoski, R. V. Skibbens, PCNA antagonizes cohesin-dependent roles in
558 genomic stability. *PLoS ONE* **15**, e0235103 (2020).
559 72. K. Tong, R. V. Skibbens, Cohesin without Cohesion: A Novel Role for Pds5 in
560 Saccharomyces cerevisiae. *PLoS ONE* **9**, e100470 (2014).
561 73. M. S. Bloom, D. Koshland, V. Guacci, Cohesin Function in Cohesion,
562 Condensation, and DNA Repair Is Regulated by Wpl1p via a Common Mechanism
563 in Saccharomyces cerevisiae. *Genetics* **208**, 111–124 (2018).
564 74. R. Ciosk, *et al.*, An ESP1/PDS1 Complex Regulates Loss of Sister Chromatid
565 Cohesion at the Metaphase to Anaphase Transition in Yeast. *Cell* **93**, 1067–1076
566 (1998).
567 75. A. Yamamoto, Pds1p is required for faithful execution of anaphase in the yeast,
568 Saccharomyces cerevisiae. *The Journal of Cell Biology* **133**, 85–97 (1996).
569 76. F. Uhlmann, F. Lottspeich, K. Nasmyth, Sister-chromatid separation at anaphase
570 onset is promoted by cleavage of the cohesin subunit Scc1. *Nature* **400**, 37–42
571 (1999).

572 77. T. M. Leissing, L. M. Luh, P. M. Cromm, Structure driven compound optimization in
573 targeted protein degradation. *Drug Discovery Today: Technologies* **37**, 73–82
574 (2020).
575 78. D. Khago, I. J. Fucci, R. A. Byrd, The Role of Conformational Dynamics in the
576 Recognition and Regulation of Ubiquitination. *Molecules* **25**, 5933 (2020).
577 79. E. Blaszczak, *et al.*, Dissecting Ubiquitylation and DNA Damage Response
578 Pathways in the Yeast Saccharomyces cerevisiae Using a Proteome-Wide
579 Approach. *Mol Cell Proteomics* **23**, 100695 (2024).
580 80. D. L. Swaney, *et al.*, Global analysis of phosphorylation and ubiquitylation cross-
581 talk in protein degradation. *Nat Methods* **10**, 676–682 (2013).
582 81. I. Litwin, *et al.*, ISW1a modulates cohesin distribution in centromeric and
583 pericentromeric regions. *Nucleic Acids Research* **51**, 9101–9121 (2023).
584 82. X. Yang, *et al.*, The ubiquitin–proteasome system regulates meiotic chromosome
585 organization. *Proc. Natl. Acad. Sci. U.S.A.* **119** (2022).
586 83. J. R. S. Newman, E. Wolf, P. S. Kim, A computationally directed screen identifying
587 interacting coiled coils from *Saccharomyces cerevisiae*. *Proc. Natl. Acad.*
588 *Sci. U.S.A.* **97**, 13203–13208 (2000).
589 84. M. Costanzo, *et al.*, A global genetic interaction network maps a wiring diagram of
590 cellular function. *Science* **353** (2016).
591 85. W. Zhang, C. H. L. Yeung, L. Wu, K. W. Y. Yuen, E3 ubiquitin ligase Bre1 couples
592 sister chromatid cohesion establishment to DNA replication in Saccharomyces
593 cerevisiae. *eLife* **6**, e28231 (2017).

594 86. K. Tong, R. V. Skibbens, Pds5 regulators segregate cohesion and condensation
595 pathways in *Saccharomyces cerevisiae*. *Proc. Natl. Acad. Sci. U.S.A.* **112**, 7021–
596 7026 (2015).
597 87. M. L. Mayer, S. P. Gygi, R. Aebersold, P. Hieter, Identification of RFC(Ctf18p, Ctf8p,
598 Dcc1p). *Molecular Cell* **7**, 959–970 (2001).
599 88. C. D'Ambrosio, G. Kelly, K. Shirahige, F. Uhlmann, Condensin-Dependent rDNA
600 Decatenation Introduces a Temporal Pattern to Chromosome Segregation. *Current*
601 *Biology* **18**, 1084–1089 (2008).
602 89. V. Guacci, E. Hogan, D. Koshland, Chromosome condensation and sister
603 chromatid pairing in budding yeast. *The Journal of cell biology* **125**, 517–530
604 (1994).
605 90. T. Eng, V. Guacci, D. Koshland, Interallelic complementation provides functional
606 evidence for cohesin–cohesin interactions on DNA. *MBoC* **26**, 4224–4235 (2015).
607 91. O. Orgil, *et al.*, A Conserved Domain in the Scc3 Subunit of Cohesin Mediates the
608 Interaction with Both Mcd1 and the Cohesin Loader Complex. *PLoS Genet* **11**,
609 e1005036 (2015).
610 92. J. Woodman, M. Hoffman, M. Dzieciatkowska, K. C. Hansen, P. C. Megee,
611 Phosphorylation of the Scc2 cohesin deposition complex subunit regulates
612 chromosome condensation through cohesin integrity. *Mol Biol Cell* **26**, 3754–3767
613 (2015).
614 93. V. Guacci, D. Koshland, Cohesin-independent segregation of sister chromatids in
615 budding yeast. *MBoC* **23**, 729–739 (2012).

616 94. R. Ciosk, *et al.*, Cohesin's Binding to Chromosomes Depends on a Separate
617 Complex Consisting of Scc2 and Scc4 Proteins. *Molecular Cell* **5**, 243–254 (2000).
618 95. M. E. Maradeo, R. V. Skibbens, Replication Factor C Complexes Play Unique Pro-
619 and Anti-Establishment Roles in Sister Chromatid Cohesion. *PLoS ONE* **5**, e15381
620 (2010).
621 96. H. Yang, Q. Ren, Z. Zhang, Cleavage of Mcd1 by Caspase-like Protease Esp1
622 Promotes Apoptosis in Budding Yeast. *MBoC* **19**, 2127–2134 (2008).
623 97. Q. Ren, L.-C. Liou, Q. Gao, X. Bao, Z. Zhang, Bir1 Deletion Causes Malfunction of
624 the Spindle Assembly Checkpoint and Apoptosis in Yeast. *Front. Oncol.* **2** (2012).
625 98. A. Varshavsky, The Ubiquitin System, Autophagy, and Regulated Protein
626 Degradation. *Annu Rev Biochem* **86**, 123–128 (2017).
627 99. I. Livneh, Y. Kravtsova-Ivantsiv, O. Braten, Y. T. Kwon, A. Ciechanover,
628 Monoubiquitination joins polyubiquitination as an esteemed proteasomal targeting
629 signal. *Bioessays* **39** (2017).
630 100. F. Chen, *et al.*, Caspase Proteolysis of the Cohesin Component RAD21
631 Promotes Apoptosis. *Journal of Biological Chemistry* **277**, 16775–16781 (2002).
632 101. D. Pati, N. Zhang, S. E. Plon, Linking Sister Chromatid Cohesion and Apoptosis:
633 Role of Rad21. *Molecular and Cellular Biology* **22**, 8267–8277 (2002).
634 102. J. M. Heidinger-Pauli, O. Mert, C. Davenport, V. Guacci, D. Koshland, Systematic
635 reduction of cohesin differentially affects chromosome segregation, condensation,
636 and DNA repair. *Curr Biol* **20**, 957–963 (2010).
637 103. M. D. Rose, F. Winston, P. Hieter, *Methods in yeast genetics* (Cold Spring Harbor
638 Laboratory Press, 1990).

639 104. M. S. Longtine, *et al.*, Additional modules for versatile and economical PCR-
640 based gene deletion and modification in Saccharomyces cerevisiae. *Yeast* **14**,
641 953–961 (1998).
642 105. M. A. Kenna, R. V. Skibbens, Mechanical Link between Cohesion Establishment
643 and DNA Replication: Ctf7p/Eco1p, a Cohesion Establishment Factor, Associates
644 with Three Different Replication Factor C Complexes. *Molecular and Cellular*
645 *Biology* **23**, 2999–3007 (2003).
646 106. M. Foiani, F. Marini, D. Gamba, G. Lucchini, P. Plevani, The B Subunit of the
647 DNA Polymerase α-Primase Complex in *Saccharomyces cerevisiae* Executes an
648 Essential Function at the Initial Stage of DNA Replication. *Molecular and Cellular*
649 *Biology* **14**, 923–933 (1994).
650 107. K. J. Livak, T. D. Schmittgen, Analysis of Relative Gene Expression Data Using
651 Real-Time Quantitative PCR and the 2−ΔΔCT Method. *Methods* **25**, 402–408
652 (2001).
653

654 Figure Legends

655 **Figure 1. Mcd1 protein levels are reduced in *eco1-203* and *rad61*Δ mutated cells.**
656 A) Flow cytometry data of DNA contents for wildtype (YPH499), *eco1-203* (YBS514), *rad61*Δ
657 (YMM808) and *eco1*Δ *rad61*Δ (YBS829) mutant cells. Log phase cultures were synchronized in
658 S phase at their respective permissive temperatures, 23°C for *eco1-203* and 30°C for wildtype
659 *eco1*Δ *rad61*Δ and *rad61*Δ mutant cells, then shifted to 37°C for 1 hr. B) Representative
660 Western Blot of Mcd1 (top panel) and Pgk1 (lower panel) protein obtained from extracts of HU-
661 synchronized wildtype, *eco1-203*, *rad61*Δ and *eco1*Δ *rad61*Δ mutant cells indicated in (A). *

662 indicates non-specific band. C) Quantification of Mcd1, normalized to Pgk1 loading controls.
663 Statistical analysis was performed using a two-tailed *t*-test. Statistical differences (*) are based
664 on a $P < 0.05$ obtained across three experiments (n=3). Error bars indicate the standard
665 deviation.
666
667 **Figure 2. *MCD1* mRNA expression is increased in *eco1*Δ *rad61*Δ double mutant**
668 **cells.** A) Flow cytometry data of DNA content for log phase wildtype (YPH499) and *eco1*Δ
669 *rad61*Δ (YBS829) double mutant cells arrested in S phase at 30°C for 3 hrs. B) Representative
670 Western Blot of Mcd1 (top panel) and Pgk1 (lower panel) protein obtained from extracts of HU-
671 synchronized wildtype and *eco1*Δ *rad61*Δ double mutant cells indicated in (A). C) Quantification
672 of Mcd1, normalized to Pgk1 loading controls. Statistical analysis was performed using a two-
673 tailed *t*-test. Statistical differences (**) are based on a $P < 0.01$ obtained across four
674 experiments (n=4). Error bars indicate the standard deviation. D) Quantification of *MCD1* mRNA
675 fold change normalized to the expression of the housekeeping gene *ALG9*. Statistical analysis
676 was performed using a two-tailed *t*-test. Statistical differences (*) are based on a $P < 0.05$
677 obtained across four experiments (n=4). Error bars indicate the standard deviation.
678
679 **Figure 3. Deletion of Ubiquitin E3 ligases *SAN1* and *DAS1* suppress the growth**
680 **defects of *eco1*Δ *rad61*Δ double mutant cells.** A) Growth of 10-fold serial dilutions of A)
681 wildtype (YPH499), *bul2*Δ (YGS277), *eco1*Δ *rad61*Δ (YBS829) and two independent isolates of
682 *eco1*Δ *rad61*Δ *bul2*Δ triple mutant cells (YGS279, YGS280); B) wildtype (YPH499), *bre1*Δ
683 (YGS309), *eco1*Δ *rad61*Δ (YBS829) and two independent isolates of *eco1*Δ *rad61*Δ *bre1*Δ triple
684 mutant cells (YGS292, YGS293); C) wildtype (YPH499), *lbd19*Δ (YGS281), *eco1*Δ *rad61*Δ
685 (YBS829) and two independent isolates of *eco1*Δ *rad61*Δ *lbd19*Δ triple mutant cells (YGS282,
686 YGS283); D) wildtype (YPH499), *san1*Δ (YGS284), *eco1*Δ *rad61*Δ (YBS829) and two
687 independent isolates of *eco1*Δ *rad61*Δ *san1*Δ triple mutant cells (YGS286, YGS287); and E)

688 wildtype (YPH499), *das1*Δ (YGS288), *eco1*Δ *rad61*Δ (YBS829) and two independent isolates of
689 *eco1*Δ *rad61*Δ *das1*Δ triple mutant cells (YGS290, YGS291). Temperature and days of growth
690 are indicated.
691
692 **Figure 4. Increased Mcd1 levels partially rescue the growth defects of cohesin**
693 **mutated cells.** A) Growth of 10-fold serial dilutions of cells (strains indicated below) that
694 contains either 2μ vector (pRS424) or 2μ vector that contains *MCD1* (pBS1476). Two
695 independent isolates are shown of mutated strains that express elevated levels of *MCD1*. Cell
696 strains are as follows: A) wildtype (YGS209, YGS210) and *smc3-42* (YGS229, YGS230,
697 YGS231); B) wildtype (YGS209, YGS210) and *smc1-259* (YGS211, YGS212, YGS213); C)
698 wildtype (YBS4558, YBS4562) and *scc3-6* (YBS4568, YBS4569); D) wildtype (YGS209,
699 YGS210) and *eco1-203* (YGS329, YGS330, YGS331); and E) wildtype (YGS216, YGS217) and
700 *scc2-4* (YGS 218, YGS219, YGS220). Temperature and days of growth are indicated. Strain
701 genotypes are provided in Supplementary Table 1.
702
703 **Figure 5. Increased Mcd1 protein levels suppress *smc1-259* cell condensation**
704 **defects.** A) Flow cytometry data of DNA content for log phase cells pre-synchronized in G1
705 phase at 23°C, then shifted to 34°C (the non-permissive temperature of *smc1-259*) in
706 nocodazole. Genotypes of wildtype (YGS335, YGS337) and *smc1-259* mutated (YGS338,
707 YGS341) cells that contain either 2μ vector (pRS424) or 2μ vector that contains *MCD1* are
708 provided in Supplementary Table 1. B) Representative micrographs of rDNA detected by Net1-
709 GFP. DNA is detected by DAPI staining. C) The percentage of cells with condensed rDNA is
710 plotted. At least 120 nuclei were scored per genotype. Statistical analysis was performed using
711 a two-tailed *t*-test. Statistical differences (ns) are based on a $P > 0.05$ obtained across two
712 experiments (n=2). Error bars indicate the standard deviation. D) The uncondensed rDNA
713 structures for all strains were further classified as either fully decondensed “puffs” or partially

714 decondensed “partial”. Statistical analysis was performed using a two-tailed *t*-test. Statistical
715 differences (**) are based on a $P < 0.01$, and (***) are based on a $P < 0.001$ obtained across
716 two experiments (n=2). Error bars indicate the standard deviation.
717
718 **Figure 6 Increased Mcd1 levels in *smc1-259* cells significantly suppresses sister**
719 **chromatid cohesion defects.** A) Flow cytometry data of DNA content as described in Figure 5.
720 B) Representative micrographs of GFP dots (markers of sister chromatid cohesion) in cell
721 treatments as described in Figure 5. Genotypes of wildtype (YGS333, YGS334) and *smc1-259*
722 mutated (YGS321, YGS323) cells modified to contain both cohesion cassettes and either 2μ
723 vector (pRS424) or 2μ vector that contains *MCD1* are provided in Supplementary Table 1. C)
724 The percentage of cells in which sisters are separated (two GFP spots indicated of a sister
725 chromatid cohesion defect) is plotted. At least 120 cells were scored for each genotype.
726 Statistical analysis was performed using a two-tailed *t*-test. Statistical differences (ns) are based
727 on a $P > 0.05$, (*) are based on a $P < 0.05$ and (**) are based on a $P < 0.01$ obtained across two
728 experiments (n=2). Error bars indicate the standard deviation.
729
730
731
732
733
734
735
736
737
738

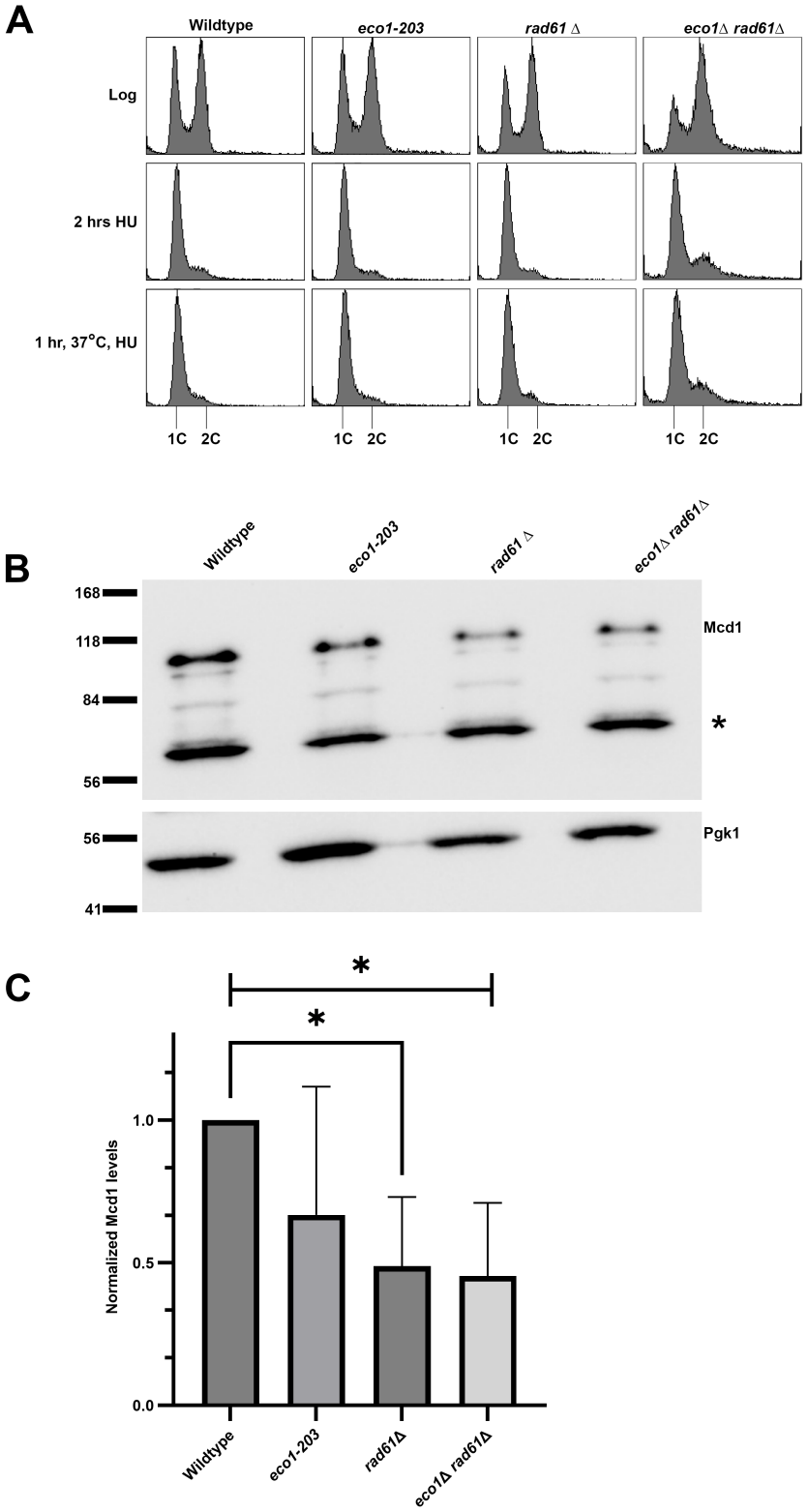
A
Wildtype
eco1-203
rad61 Δ
eco1Δ rad61Δ
Log
2 hrs HU
1 hr, 37°C, HU
1C 2C
B
Wildtype
eco1-203
rad61 Δ
eco1Δ rad61Δ
168
118
84
56
Mcd1
*
56
41
Pgk1
C
*
*
1.0
0.5
0.0
Normalized Mcd1 levels
Wildtype
eco1-203
rad61Δ
eco1Δ rad61Δ

Figure 1

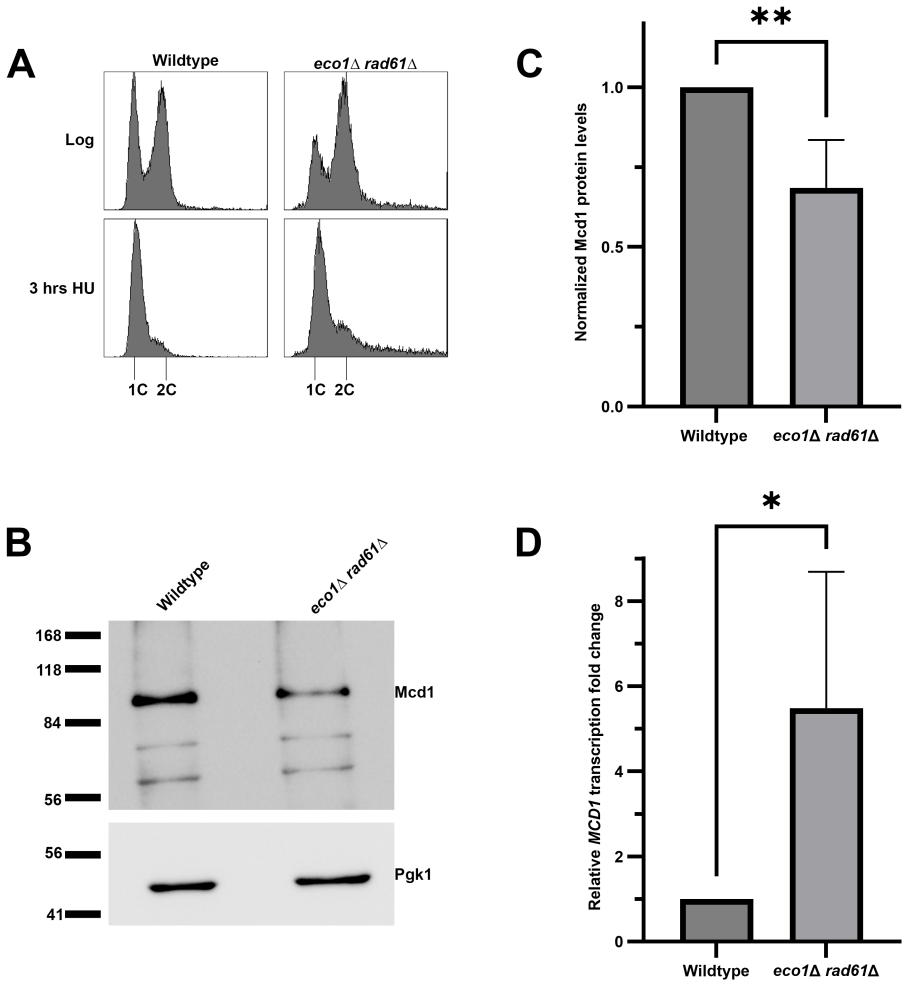

741

742

743

744

745 Figure 2

746

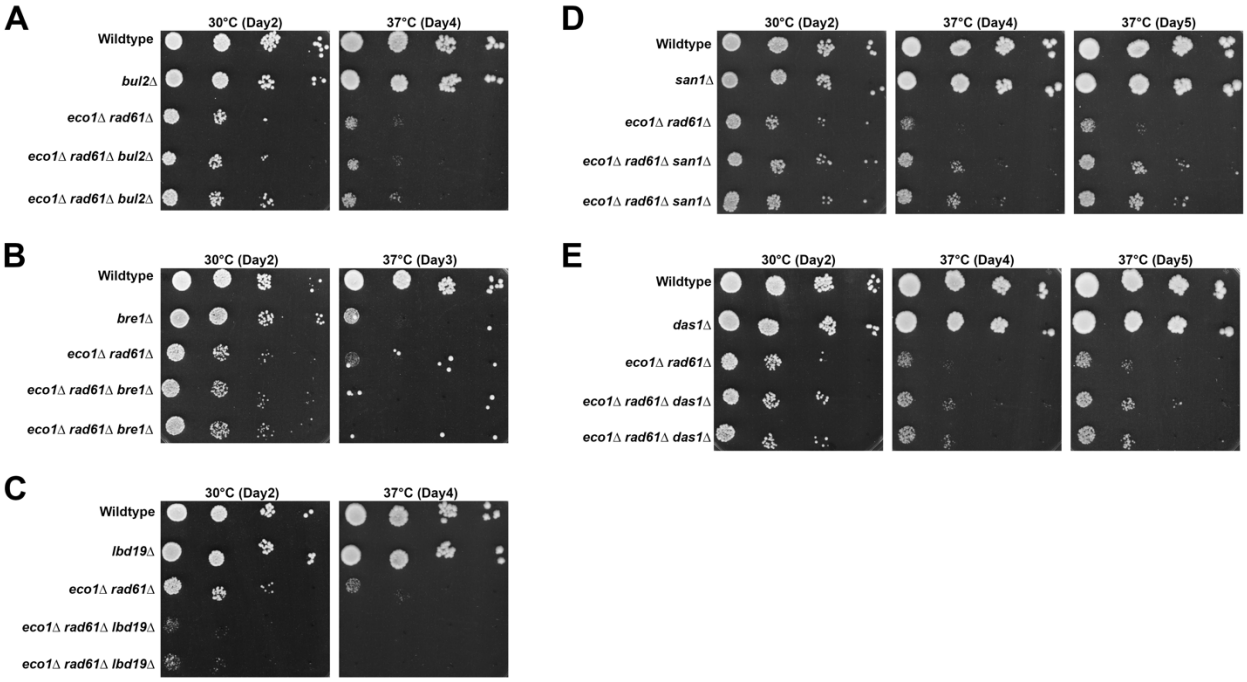
A
30°C (Day2)
37°C (Day4)
Wildtype
bul2Δ
eco1Δ rad61Δ
eco1Δ rad61Δ bul2Δ
eco1Δ rad61Δ bul2Δ
B
30°C (Day2)
37°C (Day3)
Wildtype
bre1Δ
eco1Δ rad61Δ
eco1Δ rad61Δ bre1Δ
eco1Δ rad61Δ bre1Δ
C
30°C (Day2)
37°C (Day4)
Wildtype
lbd19Δ
eco1Δ rad61Δ
eco1Δ rad61Δ lbd19Δ
eco1Δ rad61Δ lbd19Δ
D
30°C (Day2)
37°C (Day4)
37°C (Day5)
Wildtype
san1Δ
eco1Δ rad61Δ
eco1Δ rad61Δ san1Δ
eco1Δ rad61Δ san1Δ
E
30°C (Day2)
37°C (Day4)
37°C (Day5)
Wildtype
das1Δ
eco1Δ rad61Δ
eco1Δ rad61Δ das1Δ
eco1Δ rad61Δ das1Δ

Figure 3

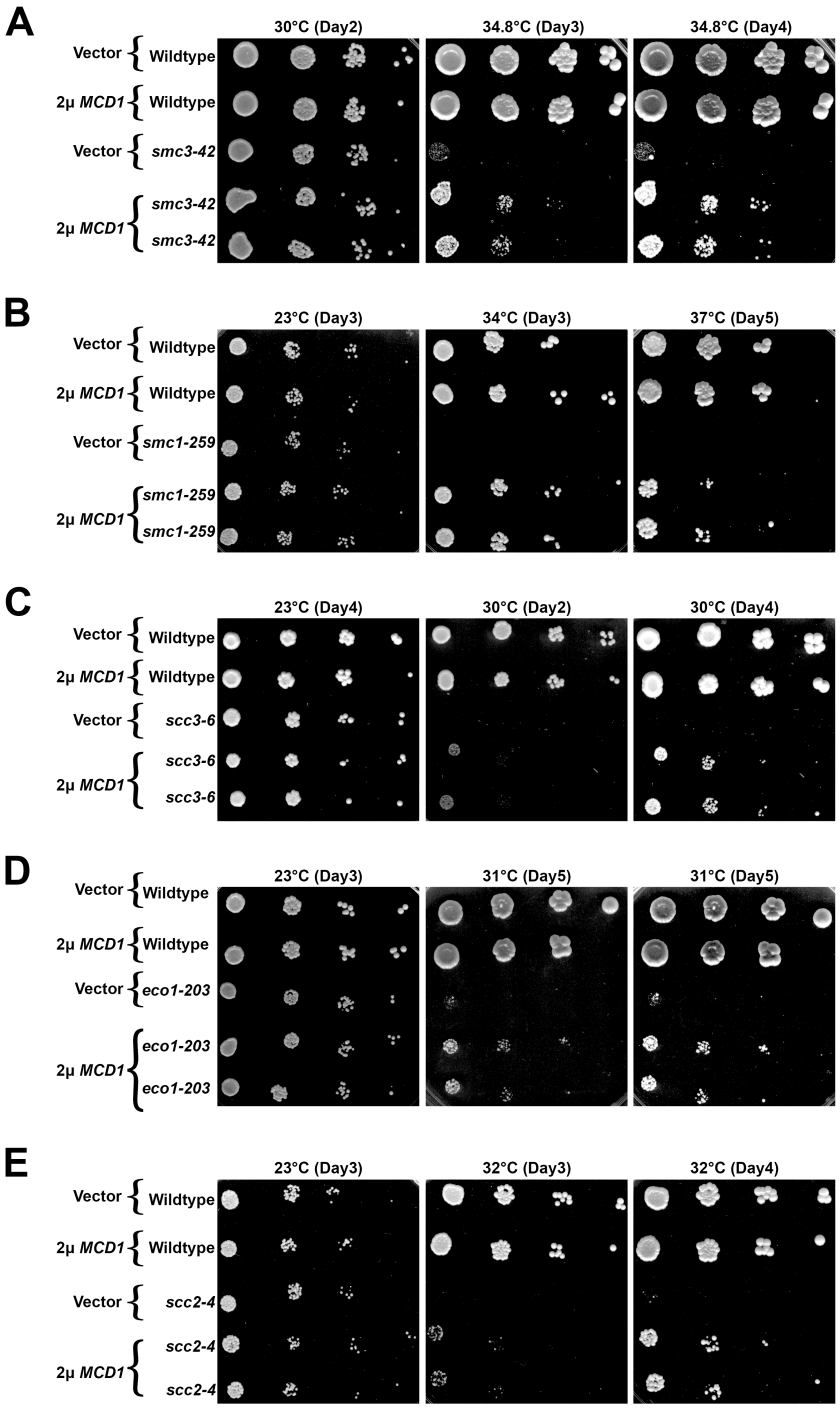

753

754

755 Figure 4

756

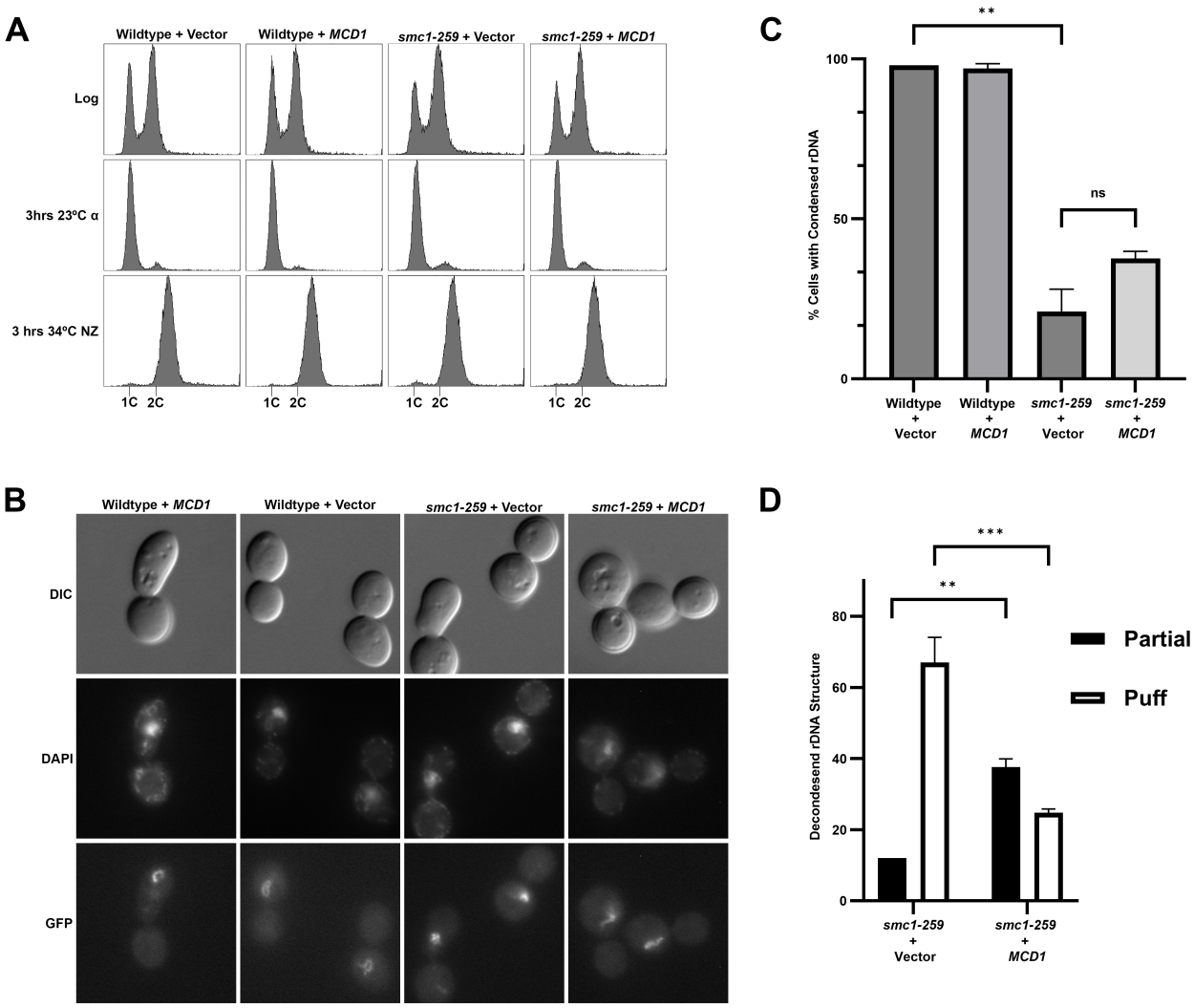

757

758

759

760 Figure 5

761

762

763

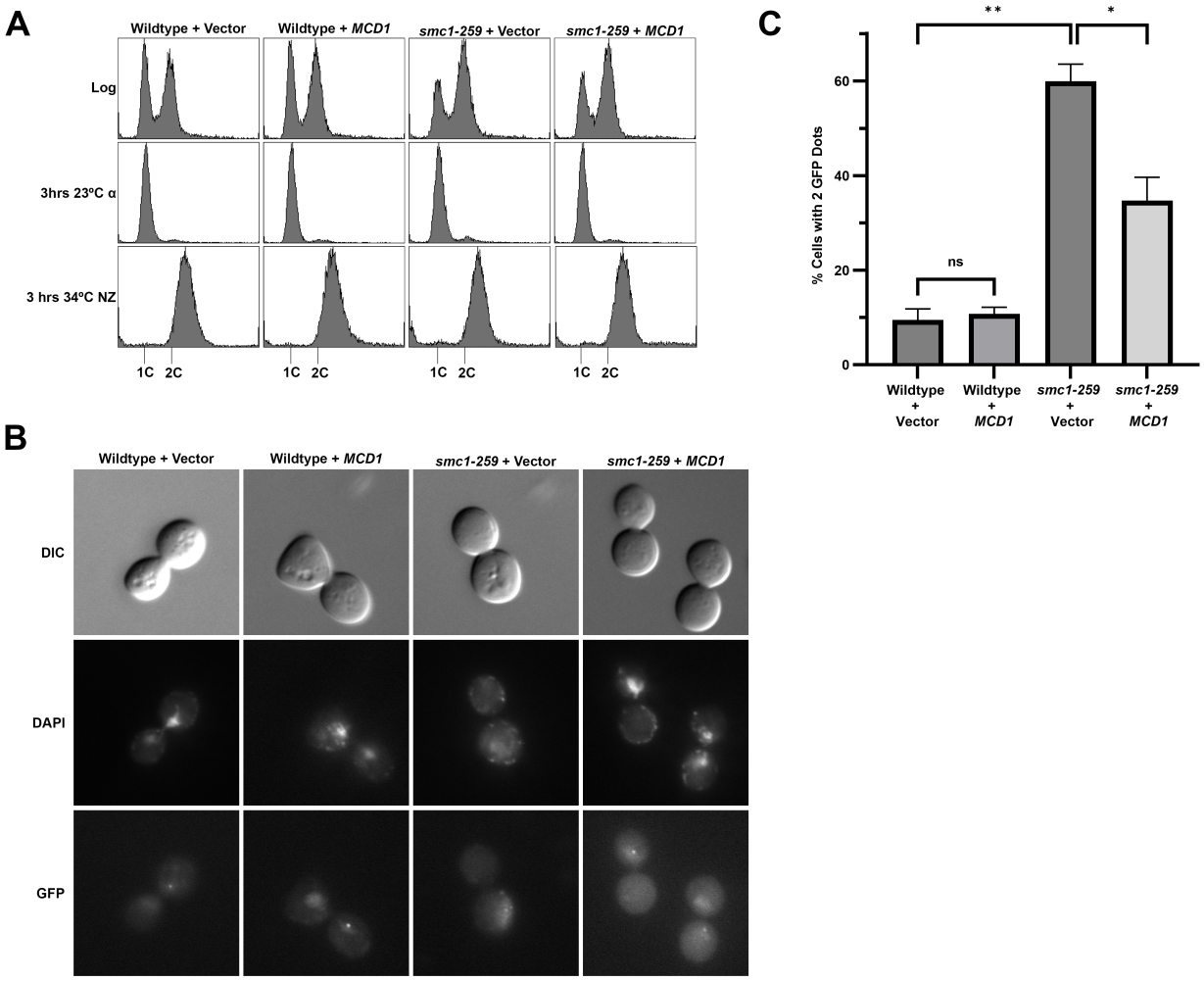
A
Wildtype + Vector
Wildtype + MCD1
smc1-259 + Vector
smc1-259 + MCD1
Log
3hrs 23ºC α
3 hrs 34ºC NZ
1C 2C
B
DIC
DAPI
GFP
C
% Cells with 2 GFP Dots
0
20
40
60
ns
**
*
Wildtype + Vector
Wildtype + MCD1
smc1-259 + Vector
smc1-259 + MCD1

Figure 6